FULL PAPER

Flexible Ru^{II} Schiff base complexes: selective G-quadruplex DNA binding and photo-induced cancer cell death

Martin Gillard,[a] Justin Weynand,[a,b] Hugues Bonnet,[b] Frédérique Loiseau,[b] Anabelle Decottignies,[c] Jérôme Dejeu*,[b] Eric Defrancq*[b] and Benjamin Elias*[a]

Abstract:
A series of new Ru^{II} Schiff base complexes built on the salphen moiety has been prepared. This includes four monometallic Ru^{II} compounds and six bimetallic analogues that contain Ni^{II}, Pd^{II} or Pt^{II} cations into the salphen complexation site. Steady state luminescence titrations illustrated the capacity of the compounds to photoprobe G-quadruplex DNA. Moreover, the vast array of the Schiff base structural changes allowed to extensively assess the influence of the ligand surface, flexibility and charge on the interaction of the compounds with G-quadruplex DNA. This was achieved thanks to circular dichroism melting assays and bio-layer interferometry studies that pointed up high affinities along with good selectivities of Ru^{II} Schiff base complexes for G4 DNA. *In cellulo* studies were carried out with the most promising compounds. An efficient cellular uptake with location of the compounds in the nucleus as well as in the nucleolus was observed. Cell viability experiments were performed with U2OS osteosarcoma cells in the dark and under light irradiation which allowed the measurements of IC_{50}'s and photoindexes. They showed the substantial role played by light irradiation in the activity of the drugs in addition to the low cytotoxicity of the molecules in the dark. Altogether, the reported results emphasize the promising properties of Ru^{II} Schiff base complexes as a new class of candidates for developing potential G4 DNA targeting diagnostic or therapeutic compounds.

Introduction

DNA has been one of the privileged cellular target in cancer research since the understanding of the nitrogen mustard gas mode of action reported in 1946.[1] Chemotherapeutics targeting DNA have proven to be extremely effective drugs and to constitute a major step forward in the survival of cancer patients. However, this class of drugs turned out to be highly cytotoxic, often resulting in heavy side effects due to the weak selectivity of the compounds towards cancer cells.[2] During the last decades, the pursuit for more selective anticancer agents has emulated the development of new drugs able to recognize non-canonical DNA substructures that are found in cancer cells such as mismatches[3-7] and G-quadruplexes (G4s).[8-9] G4s, in which DNA assembles in the stacking of at least two guanine quartets, constitute a more and more studied target as they are well differentiated from duplex DNA.[10-12] Furthermore, G4 DNA was reported to play a key role in the development of cancer being involved in the immortalisation process by virtue of their abundance in telomeric regions.[13] Indeed, reactivation of the telomerase protein in most cancer cells promotes the telomere extension in turn favoring the proliferation of cancer.[14] Therefore, G4 DNA appeared to be in higher prevalence in cancer cells, which has opened a new field for more targeted therapies.[15-17]

Plenty of small molecules have already been described for their tight binding of G4s *in vitro*; with some compounds being at advanced stages of clinical trials.[8-9] Among the designed compounds, organic molecules based either on the acridine, phenanthroline or more recently quinazoline frameworks showed good selectivities for G4;[18-22] while in terms of metal complexes, many metalloporphyrins, metal-salphens and ruthenium (II) complexes also revealed to possess high affinities and selectivities towards G4.[23-31] The common feature of these drugs lies in their rigid planar extended scaffold that gives rise to very efficient π-stacking interactions with the quadruplex.[32-33] More recently, some studies focused on the interest of designing flexible ligands for recognizing G4 DNA thanks to favored groove interactions.[34-35]

In the present paper, we report on the synthesis of four new Ru^{II} complexes **1**-**4** that contain a flexible Schiff base type ligand built on the salphen moiety (Figure 1) along with the study of the interactions of these systems with G4 DNA. The presence of the salphen moiety in complexes **1**-**3** allowed us to prepare the rigidified bimetallic analogues **5**-**10** that contain a d^8 cation (Ni^{II}, Pd^{II} or Pt^{II}) into the salphen complexation site. This was made in order to study the influence of the ligand rigidity on the G4 recognition. More generally, the studied scaffold was selected for its high structural versatility. Furthermore, as mentioned, metal-salphen are well-known G4 DNA binders; but these compounds often suffer from low water solubility that has to be promoted by charged ligands. Conversely, Ru^{II} complexes are well water soluble compounds that proved to have suitable cellular uptake properties in addition to the well-known ability to induce cellular damages under light irradiation.[36-39] Therefore, the prospect of

[a] M. Gillard, Dr. J. Weynand and Prof. B. Elias
Université catholique de Louvain (UCLouvain)
Institut de la Matière Condensée et des Nanosciences (IMCN), Molecular Chemistry, Materials and Catalysis (MOST)
Place Louis Pasteur 1, bte L4.01.02, 1348 Louvain-la-Neuve (Belgium)
E-mail: Benjamin.Elias@uclouvain.be
[b] Dr. J. Weynand, Dr. J. Dejeu, Prof. E. Defrancq
Université Grenoble Alpes (UGA)
Département de Chimie Moléculaire, UMR CNRS 5250
CS 40700 - 38058 Grenoble (France).
E-mail: eric.defrancq@univ-grenoble-alpes.fr
jerome.dejeu@univ-grenoble-alpes.fr
[c] Prof. A. Decottignies
Université catholique de Louvain (UCLouvain)
de Duve Institute
Avenue Hippocrate 75 , 1200 Brussels (Belgium)

combining selectivity towards G4 with precise irradiation techniques emphasizes the relevance of this class of compounds in the search for more targeted therapies. In here, we describe the study of the photophysics of the Ru^{II} Schiff base complexes **1**-**10** by UV-vis absorption, light emission spectroscopy and excited state lifetime measurements. Their ability to selectively bind to G4 over duplex DNA was fully studied by steady state luminescence titrations, circular dichroism studies and bio-layer interferometry analysis. Eventually, cellular uptake and localization of the compounds were determined by confocal microscopy along with their ability to induce cell death under light irradiation (IC_{50} measurements). This constitutes the first study of this type of Ru^{II} complexes in the context of G4 recognition and cellular photo-cytotoxicity assays.

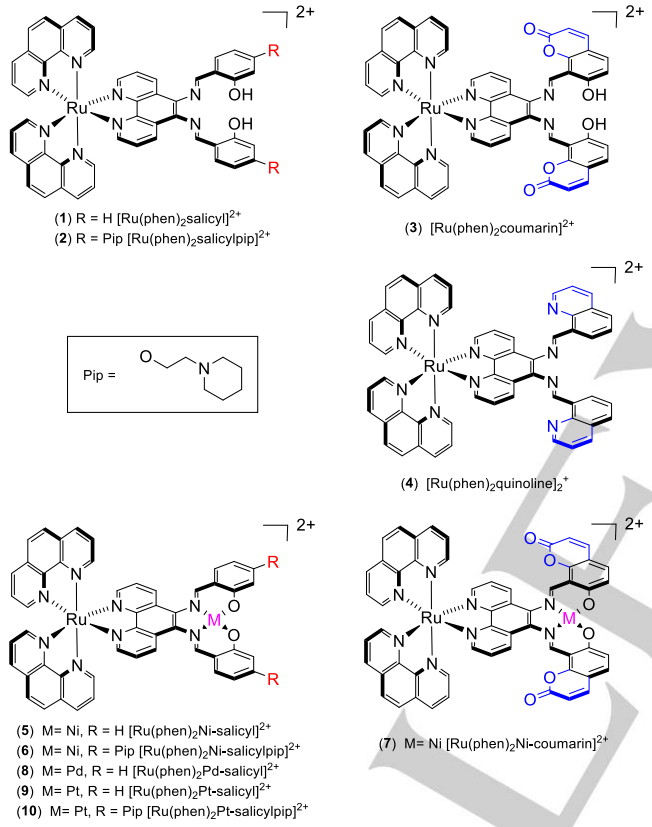

Figure 1. Structure of the Ru^{II} Schiff base complexes **1**-**10**.

Results and Discussion

Synthesis of Ru^{II} Schiff base and bimetallic d^8-analogs

The synthesis of four Schiff base type ligands was achieved by the condensation of 5,6-diamino-1,10-phenanthroline with two equivalents of the appropriate aldehyde (*i.e.* salicylaldehyde, 2-hydroxy-4-(2-(piperidin-1-yl)ethoxy) benzaldehyde, 7-hydroxycoumarin-8-carbaldehyde and 8-quinolinecarbaldehyde) in the presence of triethylamine in refluxing ethanol (yield: 38-44%, see supporting information). Salicylaldehyde and 8-quinolinecarbaldehyde were commercially available; while 7-hydroxycoumarin-8-carbaldehyde was prepared *via* the Duff formylation of 7-hydroxycoumarin and 2-hydroxy-4-(2-(piperidin-1-yl)ethoxy) benzaldehyde was prepared *via* the alkylation of 2,4-dihydroxybenzaldehyde by 1-(2-chloroethyl)piperidine (see supporting information). The structure of the ligands was confirmed by ^{1}H-NMR spectroscopy and HRMS analysis (see supporting information). The corresponding Ru^{II} complexes were synthesized by the direct chelation of the ligands onto a $[Ru(phen)_2Cl_2]$ precursor in refluxing ethanol (yield: 62-81%, see supporting information). Complexes **1**-**4** were isolated as orange powders and characterized by ^{1}H-NMR spectroscopy and HRMS analysis (see supporting information). ^{1}H-NMR spectroscopy shows unambiguously the symmetry of the compounds, which induces the equivalence of (i) the protons of the ligands and (ii) of the phenanthroline moieties.

Bimetallic analogues of complexes **1**-**3** containing a d^8 transition metal cation (Ni^{II}, Pd^{II} or Pt^{II}) into the salphen complexation site were synthesized to study the influence of the rigidity of the extended ligand on the G4 recognition capability of the compounds. Another synthesis strategy was followed for these structures by modifying the conditions described by Onozawa-Komatsuzaki *et al.* for similar compounds.[40] The key reaction consists in a one-step assembly of a $[Ru(phen)_2$5,6-diamino-1,10-phenanthroline$]^{2+}$ precursor prepared by reported method[41] with 2 eq. of the appropriate aldehyde and one equivalent of the d^8 metal cation acetate salt (see supporting information). The reactions were performed in DMSO at 100 °C in the presence of triethylamine over the course of three hours. They led to the formation of the corresponding bimetallic complexes **5-10** as dark red powders with proper yields (28-64%) (Figure 1). This synthetic pathway proved to be very convenient as it allowed the preparation of a vast array of analogs by simply changing the nature of the aldehyde or/and of the metal cation in the one pot reaction. While Ru^{II}-Ni^{II}, Ru^{II}-Cu^{II} and Ru^{II}-Zn^{II} complexes were already reported by similar methods,[40] those are to the best of our knowledge the first described syntheses of Ru^{II}-Pd^{II} and Ru^{II}-Pt^{II} salphen complexes.

Electrochemical study

To study the intrinsic photophysical properties of compounds **1**-**10**, electrochemical analyses were first implemented by cyclic voltammetry in dry deoxygenated CH_3CN (Table 1). The oxidation stage revealed very similar results for all the complexes showing a one electron oxidation wave within the investigated window, which is close to that of the Ru^{2+}/Ru^{3+} oxidation of $[Ru(phen)_3]^{2+}$ (1.32 V *vs.* Ag/AgCl). Concerning the reduction, three reversible one electron waves were detected at very similar potentials for all complexes, which were found notably easier to reduce than $[Ru(phen)_3]^{2+}$. The first reduction wave (-0.86 to -0.91 V *vs.* Ag/AgCl) is ascribed to the reduction of the imine fragments as already proposed for similar complexes.[42] The two other reduction waves are attributed to the subsequent reductions of the two phenanthroline ancillary ligands. As expected, the complexation of a metal cation (Ni^{II}, Pd^{II} or Pt^{II}) into the salphen site led to more positive potentials of the first reduction ($\Delta V \approx$ 0.07V). Altogether, systems **1**-**10** exhibit very similar electrochemical properties with data indicating that their HOMO is

located onto the Ru^{II} centre and that their LUMO is located onto the Schiff base unit of the extended ligand.

Table 1. Oxidation ($E_{1/2\ ox}$) and reduction ($E_{1/2\ red}$) potentials of complexes **1**-**10**.

Complex	$E_{1/2ox}$[a][V][b]		$E_{1/2\ red}$ [a] [V][b]	
$[Ru(phen)_3]^{2+}$	1.32	-1.30	-1.47	-1.68
$[Ru(phen)_2salicyl]^{2+}$ **1**	1.36	-0.91	-1.45	-1.64
$[Ru(phen)_2salicylpip]^{2+}$ **2**	1.36	-0.90	-1.47	-1.66
$[Ru(phen)_2coumarin]^{2+}$ **3**	1.34	-0.88	-1.43	-1.63
$[Ru(phen)_2quinoline]^{2+}$ **4**	1.33	-0.86	-1.44	-1.65
$[Ru(phen)_2Ni\text{-}salicyl]^{2+}$ **5**	1.37	-0.84	-1.45	-1.68
$[Ru(phen)_2Ni\text{-}salicylpip]^{2+}$ **6**	1.36	-0.84	-1.40	-1.69
$[Ru(phen)_2Ni\text{-}coumarin]^{2+}$ **7**	1.36	-0.81	-1.42	-1.63
$[Ru(phen)_2Pd\text{-}salicyl]^{2+}$ **8**	1.36	-0.86	-1.45	-1.62
$[Ru(phen)_2Pt\text{-}salicyl]^{2+}$ **9**	1.34	-0.87	-1.45	-1.61
$[Ru(phen)_2Pt\text{-}salicylpip]^{2+}$ **10**	1.35	-0.86	-1.44	-1.61

[a] Measured in dry acetonitrile. [b] Potentials are given *vs.* Ag/AgCl.

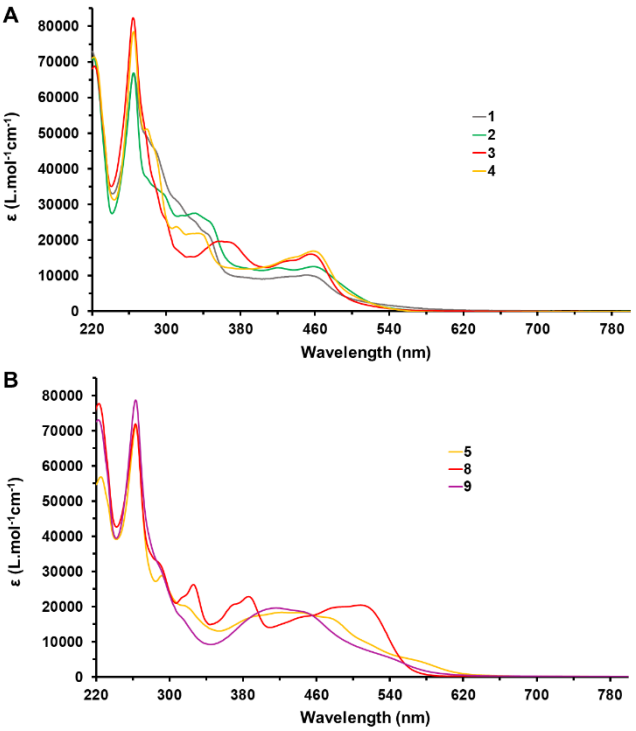

Figure 2. Absorption spectra in acetonitrile under air of A) complexes **1**-**4** and B) complexes **5**, **8** and **9**.

Light absorption

Light absorption data of the complexes were recorded at ambient temperature in water and in acetonitrile under air (Table 2). The spectra of complexes **1**-**4** display typical shapes and molar extinction coefficients of polyazaaromatic Ru^{II} complexes. Indeed, in the visible part of the spectra (at *ca.* 460 nm), we notice the occurrence of absorption bands ($\varepsilon \approx 15000$ $L.mol^{-1}cm^{-1}$) assigned to MLCT transitions. Strong absorption bands resulting from LC transitions centred on the phenanthroline ligands are also observed in the UV-region (250 nm). Noticeably, the presence of the coumarin moiety in complexes **3** and **7** leads to the apparition of a larger band at *ca.* 360 nm compared to the salicylic analogs (Figure 2 A and see supporting information). Besides, the addition of a d^8 cation into the salphen site substantially increased the absorption intensity in the visible (Figure 2 B). This is attributed to the overlay of the MCLT transitions of Ru^{II} and d^8 salphen moieties and to an increased conjugation occurring between the d^8 salphen and the phenanthroline parts of the complexes as already proposed in the literature.[40, 43-44] Interestingly, the fact that Ru^{II}-Ni^{II} analogs **5**-**7** display the most bathochromic absorption among the bimetallic analogs **5**-**10** is in accordance with their higher reduction potential. This can be correlated with the fact that the Ni^{II} cation is more electron withdrawing than Pd^{II} and Pt^{II} cations that possess larger ionic radii and higher electronic density.

Table 2. Absorption data in CH_3CN for complexes **1**-**10**.

Complex	Absorbance λ_{max} [nm] (ε [10^4 $L.mol^{-1}.cm^{-1}$])[a]
$[Ru(phen)_3]^{2+}$	265, 418 (sh), 447 (1.84)
$[Ru(phen)_2salicyl]^{2+}$ **1**	265, 288 (sh), 313 (sh), 338 (sh), 458 (1.04)
$[Ru(phen)_2salicylpip]^{2+}$ **2**	265, 296 (sh), 333 (2.71), 461 (1.28)
$[Ru(phen)_2coumarin]^{2+}$ **3**	265, 363 (1.95), 428(1.44), 457 (1.69)
$[Ru(phen)_2quinoline]^{2+}$ **4**	265, 281 (sh), 341 (sh), 433 (sh), 460 (1.71)
$[Ru(phen)_2Ni\text{-}salicyl]^{2+}$ **5**	265, 320, 428 (1.94), 454 (1.74), 580 (0.46)
$[Ru(phen)_2Ni\text{-}salicylpip]^{2+}$ **6**	265, 294, 427 (1.90), 454 (1.71), 580 (0.44)
$[Ru(phen)_2Ni\text{-}coumarin]^{2+}$ **7**	265, 294, 348 (3.77), 422 (2.18), 481 (1.76)
$[Ru(phen)_2Pd\text{-}salicyl]^{2+}$ **8**	265, 329, 389 (2.24), 478 (1.96), 514 (20.1)
$[Ru(phen)_2Pt\text{-}salicyl]^{2+}$ **9**	265, 414 (1.94), 452 (1.79), 540 (0.50)
$[Ru(phen)_2Pt\text{-}salicylpip]^{2+}$ **10**	265, 412 (1.91), 452 (1.77), 540 (0.49)

[a] Measurements were performed with 1 x 10^{-5} mol L^{-1} solutions of the complex at room temperature. Extinction coefficients are reported in brackets. sh = shoulder.

Light emission

Light emission properties of complexes **1**-**10** were investigated in acetonitrile and in water. Strong luminescence of complexes **1**-**4**

was observed with wavelengths, quantum yields and excited state lifetimes similar to those of $[Ru(phen)_3]^{2+}$ (Table 3). These typical characteristics indicate a ^{3}MLCT-type emitting state for complexes **1**-**4** as already reported for $[Ru(phen)_3]^{2+}$.[45] In addition, complexes **1**-**4** also displayed longer excited state lifetimes in water than in acetonitrile as observed for $[Ru(phen)_3]^{2+}$ which can be linked to a difference of the capability of the complex to reach the ^{3}MC non-emissive state.[45] The bimetallic Ru^{II}-Ni^{II} and Ru^{II}-Pd^{II} compounds **5**-**8** were very poorly luminescent with short lifetimes (4-44 ns) and low emission quantum yields (*i.e.* $<10^{-5}$). This is in agreement with the few similar bimetallic Ru^{II}-Ni^{II} complexes reported in the literature and is attributed to an electron transfer through the metal-salphen fragment in turn leading to luminescence quenching.[40, 46] The luminescence of the compounds being crucial to perform biological assays, it was of high importance to obtain luminescent bimetallic analogs. This encouraged us to synthesize a series of Ru^{II}-Pt^{II} analogs. Interestingly, the Ru^{II}-Pt^{II} compounds **9** and **10** showed much stronger luminescence than the Ru^{II}-Ni^{II} and Ru^{II}-Pd^{II} analogs. As already proposed for the monometallic Pt^{II} salphen complexes, the involved transition likely consists in a triplet metal-ligand to ligand charge transfer (MLLCT) occurring between the Pt^{II} phenoxide moiety and the imine fragments (Pt(d)/O(p)→ π∗(N^N)).[43-44] This assumption is supported by the fact that complexes **9** and **10** possess very similar photophysical properties thanthose of Pt^{II} salphen complexes with (i) very close emission wavelength maxima (λ = 641-644 nm in acetonitrile) and (ii) the same characteristic large hypsochromic shift of the emission maxima from acetonitrile to water (Δλ ≈ 25 nm). This increase of the luminescence energy in a more polar solvent suggests that Ru^{II}-Pt^{II} complexes are less polar at the excited state than at the ground state.

Table 3. Emission data in CH_3CN and H_2O at 298 K under ambient air for complexes **1**-**10**.

Complex	Emission λ_{max}[a,b][nm]		Φ_{em}[c,d]		τ[c] [ns]		k_r [10^3 s^{-1}]	
	CH_3CN	H_2O	CH_3CN	H_2O	CH_3CN	H_2O	CH_3CN	H_2O
$[Ru(phen)_3]^{2+}$	604	606	0.028	0.072	460	920	60.9	75.0
$[Ru(phen)_2salicyl]^{2+}$ **1**	599	600	0.018	0.075	688	1222	26.2	61.4
$[Ru(phen)_2salicylpip]^{2+}$ **2**	599	600	0.022	0.081	687	1210	32.0	66.9
$[Ru(phen)_2coumarin]^{2+}$ **3**	599	601	0.019	0.065	576	862	33.0	75.4
$[Ru(phen)_2quinoline]^{2+}$ **4**	598	600	0.032	0.092	670	1080	47.8	85.2
$[Ru(phen)_2Ni\text{-}salicyl]^{2+}$ **5**	680	n.d.	—[e]	—[e]	7	n.d.	n.d.	n.d.
$[Ru(phen)_2Ni\text{-}salicylpip]^{2+}$ **6**	678	n.d.	—[e]	—[e]	5	n.d.	n.d.	n.d.
$[Ru(phen)_2Ni\text{-}coumarin]^{2+}$ **7**	682	n.d.	—[e]	—[e]	4	n.d.	n.d.	n.d.
$[Ru(phen)_2Pd\text{-}salicyl]^{2+}$ **8**	670	n.d.	—[e]	—[e]	44	n.d.	n.d.	n.d.
$[Ru(phen)_2Pt\text{-}salicyl]^{2+}$ **9**	644	619	0.0041	0.0068	380	460	14.8	8.04
$[Ru(phen)_2Pt\text{-}salicylpip]^{2+}$ **10**	641	618	0.0037	0.0066	352	458	19.6	8.95

[a] Measurements were made with solutions 5×10^{-6} mol L^{-1} in complex under air. [b] λ_{exc} = 450 nm. [c] Measurements were made with 5×10^{-6} mol L^{-1} solutions of the complex under nitrogen. [d] Measurements relative to $[Ru(bpy)_3]^{2+}$ in nitrogen purged aqueous solution (Φ_{em} = 0.063) and in nitrogen purged acetonitrile (Φ_{em} = 0.094); errors are estimated as 5%.[47] [e] The luminescence was observed with $\Phi_{em} < 10^{-5}$. n.d. stands for not determined.

DNA interaction studies

To investigate the ability of the compounds to bind tightly and selectively to the G-quadruplex topologies (G4s), their interaction with both duplex and G4 DNA was studied *via* steady state luminescence titrations, circular dichroism and bio-layer interferometry analyses.

Steady state luminescence titrations

The ability of the luminescent complexes **1**-**4** and **9**-**10** to photoprobe duplex and G4 DNA was first studied by steady state luminescence titrations using a 20-mer hairpin ($^{5'}$CGT$_3$CGT$_5$ACGA$_3$CG$^{3'}$) (HP$_{ATGC}$) as duplex model and the human telomeric wtTel23 sequence ($^{3'}$TT(GGGATT)$_3$GGG$^{5'}$) as G4 model. All the studied Ru^{II} Schiff base complexes displayed increased luminescence in the presence of small concentrations of duplex and G4 DNA which had not been reported for these types of systems. This behavior indicates strong binding towards these structures along with efficient protection of the excited state from non-radiative deexcitation sources (collisions with solvent, oxygen photosensitization,…) when interacting with oligonucleotides. This can be related to a "light switch" type effect as reported for the detection of duplex DNA in the case of [Ru(bpy)$_2$dppz]$^{2+}$.[48] Complexes **1** and **3** appeared to be the most promising compounds according to luminescence titrations as they exhibit a stronger enhancement of their luminescence in the presence of G4 compared to duplex DNA (Figure 3 for complex **3**, see supporting information for the other complexes), probably arising from a different protection of the complex from non-radiative deexcitation sources. Moreover, the fact that lower concentrations of complexes **1** and **3** are required to reach the light emission maximum intensity in the case of G4 oligonucleotides may indicate a stronger binding of these complexes towards G4s. The excited state of Ru^{II}-Pt^{II} Schiff base complexes **9** and **10** showed to be rather influenced by the presence of G4 compared to duplex DNA. Indeed, a notable hypsochromic shift of the emission maximum occurs while interacting with G4 DNA ($\Delta\lambda$ = 18 nm for G4 compared to 6 nm for duplex DNA) due to the more hydrophobic environment afforded by the nucleic bases.

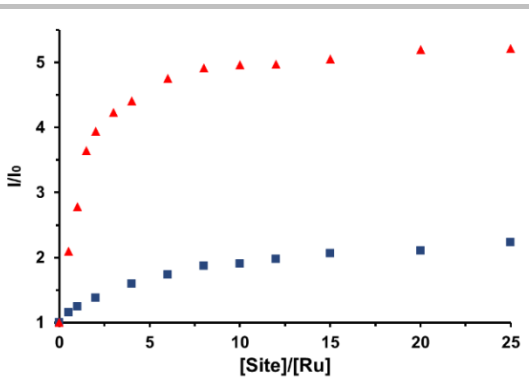

Figure 3. Relative luminescence intensity (I/I$_0$) of **3** as a function of the relative oligonucleotide concentration ([site]/[Ru]). With I$_0$, the luminescence of the complex in the absence of DNA (λ_{exc} = 450 nm). Measurements were performed using 5 µM of the complex in 10 mM HEPES (pH 7.4), 50 mM NaCl, 100 mM KCl under ambient air conditions. Site = G-quartet or base pair. Red triangles stand for wtTel23 and blue squares for HP$_{ATGC}$.

Circular dichroism

CD melting assays were implemented to further investigate the impact of the complexes **1**-**10** binding on the stability of the duplex and G4 DNA structures. CD analyses were performed using the same telomeric wtTel23 sequence as G4 model in 10 mM Tris-HCl,100 mM NaCl and using the same DNA hairpin HP$_{ATGC}$ as for luminescence titrations in 100 mM NaCl buffer. The proper folding of wtTel23 into the antiparallel G4 topology was indicated by the presence of two positive peaks at 242 and 294 nm in the 100 mM NaCl buffer (see supporting information).[49-50] The folding of HP$_{ATGC}$ was characterised by a negative peak at 252 nm.

CD melting assays were carried out to study the impact of the presence of the complex on the stability of the G-quadruplex and the hairpin DNA structures. CD melting curves were recorded in the presence (5 equivalents) and in the absence of the complex in 100 mM NaCl containing buffer for wtTel 23 and for the duplex hairpin on the temperature range 20-95°C (Table 4). The measured melting temperatures clearly show a stabilization of the G4 structure by the complexes with ΔT_m ranging from 5.1 to 10.3 °C. Interestingly, the stabilisation of G4s was found less effective with bimetallic compounds compared to monometallic ones. Indeed ΔT_m from 9 to 10.3 °C were observed for complexes **1-3** whereas for bimetallic complexes **5-10** slightly lower ΔT_m were obtained (from 5.1 to 8.6 °C). The effect of the piperidine arms was also noticed as a slight increase of ΔT_m was observed from **1** to **2**, from **5** to **6** and from **9** to **10**, respectively. Remarkably, complexes **1** and **3** displayed much weaker stabilizing effect on

Table 4. Melting temperatures (T_m) for the wtTel23 G4 and the HP$_{ATCG}$ hairpin oligonucleotides in the absence or in the presence of 5 eq of the complexes.[a]

Oligonucleotide		No complex	**1**	**2**	**3**	**4**	**5**	**6**	**7**	**8**	**9**	**10**
wtTel23	T_m [°C][b]	50.2	59.2	60.1	60.5	58.8	57.1	57.9	55.3	56.8	56.7	58.8
	Δ *Tm* [°C][c]	0	9	9.9	10.3	8.6	6.9	7.7	5.1	6.6	6.5	8.6
HP$_{ATGC}$	T_m [°C][b]	54.2	54.6	61.3	56.3	59.6	59.2	62.6	58.3	60.0	60.9	63.0
	Δ *Tm* [°C][c]	0	0.4	7.1	2.1	5.4	5.0	8.4	4.1	5.8	6.7	8.8

[a] Oligonucleotides were first annealed by heating at 95 °C for 5 min in Tris-HCl buffer (10 mM, pH 7.4) with 100 mM NaCl and then allowed to cool to room temperature overnight. Oligonucleotide concentrations were fixed at 2.5 µM. The ellipticity was recorded at 294 and 252 nm for wtTel23 and duplex hairpin, respectively. [b] Error in T_m is estimated to 0.5 °C. [c] Error on Δ Tm is estimated to 1 °C.

duplex DNA than on G4 DNA which is in accordance with the differences observed by luminescence titrations. However, it should be noticed that circular dichroism analyses as well as steady state luminescence titrations are not the most appropriate methods for the direct measurements of affinity constants with G-quadruplex DNA.[51] Therefore, bio-layer interferometry was used to determine the thermodynamic parameters of the interaction.

Bio-layer interferometry

Bio-layer interferometry analysis (BLI) is an optical technique that has been recently implemented to study biomolecular interactions between small molecules and different DNA secondary structures such as mismatches and G-quadruplexes.[7, 31, 52-53] In this study, BLI analysis was performed for complexes **1**-**10** using wtTel23 and a GC rich hairpin duplex ($^{3'}(GC)_4TTTT(GC)_4{}^{5'}$) ($HP_{GC}$) sequences which are both 3'-biotinylated for attachment on the BLI sensors.

Affinities of complexes **1**-**10** for G4s cover two orders of magnitude of concentrations (from 0.24 µM for the most affine complex **6** to 21 µM for the less affine complex **1**) showing the substantial impact of the Schiff base part structural changes on the interaction strength (Table 5 and see supporting information). The addition of positively charged piperidine chains on the salphen moiety increased significantly the affinity for G4 and appears when comparing the G4 affinity of complex **1** *versus* **2** (21 µM and 1 µM**,** respectively), complex **5** *versus* **6** (11 µM and 0.24 µM, respectively) and to a lesser extent complex **9** *versus* **10** (0.84 µM and 0.63 µM, respectively). This can be explained by favourable interactions with the G4 grooves as previously reported for metal salphen complexes.[26-29] These results were in accordance with CD melting experiments.

Replacing the salicyl moiety by the coumarin or quinoline moieties in complexes **3** and **4**, respectively, allowed an enhancement of the affinity for G4. This observation can be justified by a higher π-stacking interactions through the aromatic coumarin and quinoline part relative to the salicyl one. It was noted that the stiffening of the systems *via* the addition of Ni^{II}, Pd^{II} and Pt^{II} in the salphen moiety led to improved affinities for G4s. Indeed, bi-metallic complexes **5**, **8** and **9** showed an affinity of 11, 6.5 and 0.84 µM, respectively whereas the parent complex **1** has an affinity of 21 µM. The same trend was observed for complexes **6** and **10** (affinity for G4s of 0.24 µM and 0.63 µM, respectively) in comparison with the parent complex **2** (1.0 µM). Interestingly, the affinity for G4 also seems to follow the trend of the cation size with the Pt^{II} version **9** showing the highest affinity towards G4 (840 nM). A significant selectivity of complexes **1** and **3** for G4 relative to duplex DNA was observed. Despite an interesting increase of affinity for G4, a selectivity decrease was observed for the bi-metallic analogues. It was also noticed that although the presence of piperidine arms on the salphen fragment led to remarkable affinities towards G4 a loss of the selectivity occurred. This is likely due to increased non-specific electrostatic interactions caused by the protonation of the piperidine fragments at pH 7.4.

Finally, it is also interesting to compare the kinetic constants of the interaction between the complexes **1**-**10** for G4 and duplex DNA to better understand the observed affinity differences (Figure 4). We observed that the dissociation rates span on a larger range (from $8{,}11.10^{-2}$ s^{-1} to $2{,}2.10^{-3}$ s^{-1}) than the association rates (from $1{,}6.10^{4}$ $M^{-1}.s^{-1}$ to $1{,}8.10^{5}$ $M^{-1}.s^{-1}$). We could notice that the better affinities towards G4 relative to duplex DNA of complexes **1**, **3**, **7** and **8** was due to a slower dissociation with G4. Second, the non-selective complexes **6**, **9**, **10** display the lowest dissociation constants both for duplex and G4 DNA. Whereas complexes **2**, **4** and **6** possess the highest association rate.

Table 5. Equilibrium dissociation constants (K_D) for the interaction of complexes **1**-**10** with G4 and duplex DNA.

Complex	HP	wtTel 23
	K_D (µM)[a]	K_D (µM)[a]
$[Ru(phen)_2salicyl]^{2+}$ **1**	n.d.[b]	21 ± 2
$[Ru(phen)_2salicylpip]^{2+}$ **2**	1.0 ± 0.2	1.0 ± 0.02
$[Ru(phen)_2coumarin]^{2+}$ **3**	48 ± 11.7	2.5 ± 0.9
$[Ru(phen)_2quinoline]^{2+}$ **4**	3.9 ± 0.8	1.5 ± 0.1
$[Ru(phen)_2Ni\text{-}salicyl]^{2+}$ **5**	16 ± 7	11± 0.7
$[Ru(phen)_2Ni\text{-}salicylpip]^{2+}$ **6**	0.37 ± 0.03	0.24 ± 0.02
$[Ru(phen)_2Ni\text{-}coumarin]^{2+}$ **7**	14 ± 6	3.8 ± 0.9
$[Ru(phen)_2Pd\text{-}salicyl]^{2+}$ **8**	18 ± 1	6.5 ± 0.4
$[Ru(phen)_2Pt\text{-}salicyl]^{2+}$ **9**	1.0 ± 0.1	0.84 ± 0.2
$[Ru(phen)_2Pt\text{-}salicylpip]^{2+}$ **10**	1.4 ± 0.1	0.63 ± 0.04

[a] Equilibrium dissociation constants were deduced from the kinetic rate constants. [b] Due to the very low binding of the complex with hairpin DNA, the kinetics of the interaction could not be determined (n.d.) in the studied concentration range. Measurements were performed using a concentration range from 0.5 µM to 10 µM of the complexes in 10 mM HEPES pH 7.4, 50 mM NaCl, 100 mM KCl, 0.5% v/v surfactant P20.

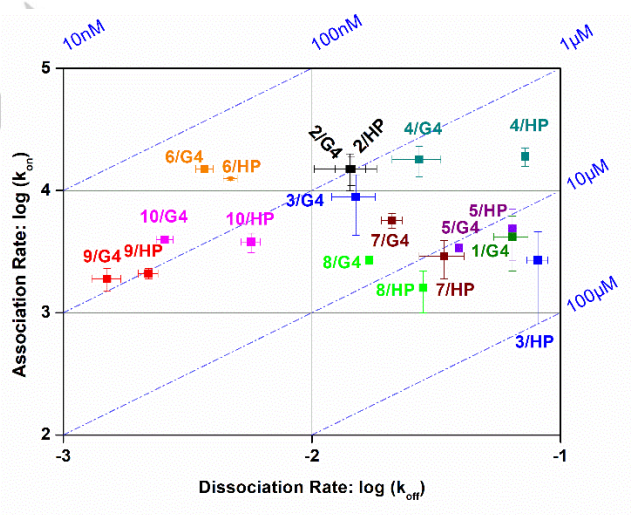

Figure 4. Two-dimensional isoaffinity kinetic plot of rate constants measured by BLI. The dashed diagonals depict the equilibrium binding constants and are shown to help with the visualization of the affinity distribution. Complexes **1-10** are plotted in the presence of duplex DNA hairpin (HP) and G4 DNA (G4). Measurements are performed using 0.5 to 10 nM of the complex in 10 mM HEPES (pH 7.4), 50 mM NaCl, 100 mM KCl and 0.5% v/v surfactant P20 under ambient air conditions.

***In cellulo* studies**

Cell penetration

Due to their promising luminescence properties, the ability of complexes **1**-**3**, **9** and **10** to penetrate cells and to target the genetic material was studied by confocal microscopy using U2OS osteosarcoma cell line as model. The selected compounds allowed to study the impact of the coumarin and the piperidine moieties and of the chelated Pt^{II} onto the cell localization of the drugs. Complexes **1-3**, **9** and **10** were found to efficiently penetrate cells with slightly distinct intracellular localization (see supporting information). Noticeably, the presence of piperidine fragments such as in complexes **2** and **10** led to enhanced ability of the complexes to target DNA *in cellulo*. Figure 5 unambiguously shows a better co-localization of compound **2** with the nucleus marker DRAQ5 compared to compound **1**. Also, complex **2** appeared to accumulate in the nucleoli, which display high density of nucleic acids (Figure 5; E). Similar observations were made for complex **10** (see supporting information). This increased targeting of complex **2** towards the genetic material is likely due to the additional positive charge brought by the piperidine arms that are protonated in biological conditions.

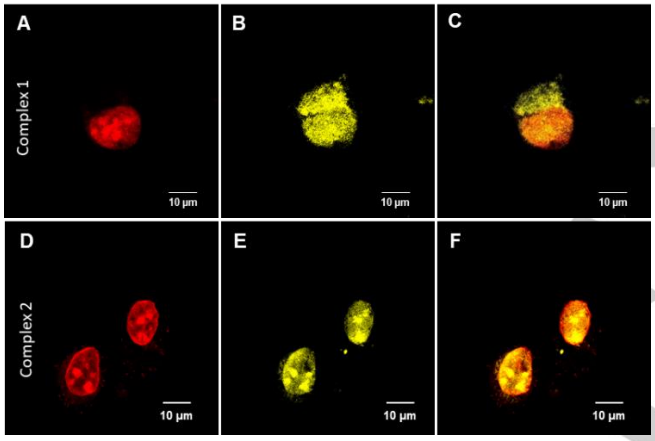

Figure 5. Cell penetration study. Confocal microscopy pictures of U2OS cancer cells after incubation with 20 µM of complex **1** (A-C) or **2** (D-F) in DMEM for 1,5 hour. Nucleus was stained in red by DRAQ5; Ru^{II} complexes appear in yellow. C and F are merged images. Scale bar 10 µm.

Cellular photo-cytotoxicity

In view of the ability of compounds **1-3**, **9** and **10** to penetrate cells and to locate in the nucleus, their ability to kill cells under light irradiation was studied using the same U2OS cancer cell line. The half maximal concentration of each complex required to kill U2OS cells (IC_{50}) was measured in the dark and under light irradiation by testing a range of concentrations. Cells were incubated with drugs for one hour, before light irradiation for 30 minutes. Control cells were not irradiated. Cells were then incubated in culture medium for 24 hours before their metabolic activity was measured to quantify cell viability. Whereas toxicity was very low in the dark for all tested compounds, cell viability decreased dramatically under light irradiation (405 nm; 15.7 Wm^{-2}) for complexes **1-3**, **9** and **10,** displaying IC_{50} values in the micromolar range or lower (Table 6). Interestingly, incorporation of piperidine arms to our systems such as in complexes **2** and **10** led to increased photo-cytotoxicities, which might be related to their increased ability to target the genetic material as suggested by the cell penetration assays. However, both compounds also showed higher toxicity in the dark (Table 6). Presence of Pt^{II} into the salphen site of compounds **9** and **10** led to very similar IC_{50} values compared to their respective non d^8 metallated analogs, complexes **1** and **2** respectively.

In conclusion, all tested compounds display high photoindex, highlighting the prominence of light excitation for the activation of the drugs as well as their remarkably weak cytotoxicity in the dark (Table 6).

Table 6. IC_{50} values of the complexes determined from dose-dependent growth inhibitory curves *vs.* U2OS cancer cell line under irradiation and in the dark.

Complex	IC_{50} value[a] [µM] Light (Dark)	PI[b]
$[Ru(phen)_2salicyl]^{2+}$ **1**	2.1 ± 0.6 (>100)	> 47
$[Ru(phen)_2salicylpip]^{2+}$ **2**	0.33 ± 0.06 (47 ± 7)	142
$[Ru(phen)_2coumarin]^{2+}$ **3**	1.4 ± 0.2 (>100)	> 71
$[Ru(phen)_2Pt\text{-}salicyl]^{2+}$ **9**	2.7 ± 0.6 (>100)	> 37
$[Ru(phen)_2Pt\text{-}salicylpip]^{2+}$ **10**	0.73 ± 0.20 (33 ± 7)	45

[a] IC_{50} values are means ± standard errors calculated from 3 independent experiments (4 wells per condition). [b] PI = photoindex = IC_{50} dark/IC_{50} light

Conclusions

In this paper, we reported on the synthesis of ten new Ru^{II} Schiff base complexes **1-10**. The structures of these compounds were inspired by the metal-salphen and the polyazaaromatic Ru^{II} complexes developed for G4 recognition and are distinct from the Ru^{II} compounds usually described in the field. We prepared bimetallic Ru^{II}-Pt^{II} salphen based complexes **9** and **10** that both showed strong luminescence in addition to photophysical properties that indicate an excited state centred on the Pt^{II} salphen moiety. The luminescence of complexes **1-4**, **9** and **10** increases significantly in the presence of DNA with complexes **1** and **3** showing well differentiated behavior in the presence of G4 relative to duplex DNA. Interestingly complexes **9** and **10** also revealed luminescence wavelength maxima that are well different between duplex and G4 DNA. The interaction of the complexes with duplex and G4 DNA was studied thanks to melting assays using circular dichroism. The presence of the d8 cation in the salphen complexation site led to weaker stabilization of G4. More generally, the results obtained could confirm the observations made in luminescence titrations with notably complexes **1** and **3** leading to stronger stabilizing effect on G4 than on duplex DNA. Finally, bio-layer interferometry was implemented to better characterize the kinetics and the strength of the interaction of the complexes with the two type of DNA secondary structures. This analysis show that the compounds interact with dissociation constants in the micromolar range or lower. Interestingly, it was noticed that the presence of the d8 cation into the salphen site of complexes **5-10** led to higher affinity for G4 DNA than their monometallic analogs **1-4**. Moreover, the monometallic complexes **1** and **3** proved to be selective for G4 DNA compared

to duplex DNA. All combined with the stronger stabilizing effect induced by complexes **1-4** on G4 recorded by CD experiments, these results could be explained by the fact that complexes that possess a more flexible interacting part give rise to a different mode of interaction with G4 DNA. Also, the presence of piperidine arms in complexes **6** and **10** led to stronger interactions with both duplex and G4 DNA, probably due to the additional charge brought by the piperidine that are protonated at pH 7.4. *In cellulo* studies were conducted using the U2OS osteosarcoma cell line to assess the ability of the molecules to penetrate the cell and to induce mortality under light irradiation. Confocal microscopy showed that all the studied complexes **1-3**, **9** and **10** penetrate the cell quickly and efficiently and mainly localize to the nucleus. Cell viability experiments conducted either in the dark or under light irradiation revealed suitable IC_{50}'s of the compounds (from 0.326 to 2.71 µM) along with high photoindex, showing the strong impact of light excitation in the activity of the drugs as well as the remarkably weak toxicity of the compounds in the dark. However, the link between the targeting of the drugs to specific DNA secondary structures and the observed cytotoxicity still needs to be established and will be a challenging project for the future. In any case, the Ru^{II} Schiff base scaffold proves to be promising in terms of theranostic applications according to luminescence, interactions and *in cellulo* studies.

Experimental Section

Materials and instrumentation

5,6-diamino-1,10-phenanthroline, $[Ru(phen)_2Cl_2]$ and $[Ru(phen)_2$5,6-diamino-1,10-phenanthroline$]^{2+}$ were synthesized according to previously described literature protocols.[41] The oligonucleotides wtTel23 ($3'$TT(GGGATT)$_3$GGG$5'$), mixed AT-GC hairpin duplex sequence HP_{ATGC} ($3'$CGT$_3$CGT$_5$ACGA$_3$CG$5'$) and GC-rich hairpin duplex HP_{GC} ($3'$(GC)$_4$TTTT(GC)$_4$$5'$) were prepared by standard automated solid phase oligonucleotide synthesis on a 3400 DNA synthesizer. After purification by RP-HPLC, they were thoroughly desalted by size-exclusion chromatography (SEC). All solvents and reagents for the synthesis were of reagent grade and were used without any further purification. All solvents for the spectroscopic and electrochemical measurements were of spectroscopic grade. Water was purified with a Millipore Milli-Q system. ^{1}H and ^{13}C NMR spectra were measured from solutions in $CDCl_3$, d_6-DMSO, CD_3OD or CD_3CN on a Bruker AC300 Avance II (300 MHz) or a Bruker AM-500 (500 MHz) spectrometer at 20 °C. Chemical shifts (in ppm) were referenced to the residual peak of the solvent as an internal standard. High-resolution mass spectra (HRMS) were recorded on a Q-extractive Orbitrap spectrometer from Thermo-Fisher, using reserpine as an internal standard. Samples were ionized by electrospray ionization (ESI; capillary temperature 320 °C, vaporizer temperature 320 °C, sheath gas flow rate 5 mL min^{-1}).

Synthesis procedures and characterization

Preparation of $[Ru(phen)_2$salicyl$]^{2+}$ 1.
The dichloro precursor $[Ru(phen)_2Cl_2]$ (20 mg, 0.038 mmol) and the salicylsalphen ligand (16 mg, 0.038 mmol) were mixed in a solution of absolute ethanol. The reaction medium was then stirred at 80 °C until the precursor was consumed as monitored by TLC. Afterwards, ethanol was evaporated and addition of small portions of NH_4PF_6 yielded to the formation of a precipitate. After centrifugation, the crude solid was washed several times with water and was then dried under reduced pressur. The residue was finally purified by flash chromatography on silica gel (CH_3CN/H_2O/ KNO_{3sat} 10:1:1/4) to provide the title compound **1** as an orange solid (35 mg, 0.030 mmol, 80%). R_f 0.31 (CH_3CN/H_2O/ KNO_{3sat} 10:1:1/4). The counter-anion exchange from PF_6 to Cl was performed by adding small portions of NBu_4Cl to a solution of the complex in acetone. **^{1}H NMR (CD_3CN, 500 MHz)** δ 9.03 (broad m, 4H, ***H$_d$*** and ***H$_c$***), 8.62 – 8.60 (m, 2H, ***H$_2$*** or ***H$_9$***), 8.60 – 8.58 (m, 2H, ***H$_2$*** or ***H$_9$***), 8.25 (s, 4H, ***H$_5$*** and ***H$_6$***), 8.12 – 8.06 (m, 4H, ***H$_7$*** and ***H$_e$***), 8.02 (dd, *J* = 5.2, 1.2 Hz, 2H, ***H$_4$***), 7.99 (dd, *J* = 5.3, 1.2 Hz, 2H, ***H$_a$***), 7.68 (dd, *J* = 8.3, 5.3 Hz, 2H, ***H$_b$***), 7.63 (d, *J* = 5.2 Hz, 2H, ***H$_3$*** or ***H$_8$***), 7.61 (d, *J* = 5.2 Hz, 2H, ***H$_3$*** or ***H$_8$***), 7.51 – 7.44 (m, 2H, ***H$_g$***), 7.17 – 7.06 (m, 4H, ***H$_f$*** and ***H$_h$***). **HRMS-ESI** calculated for $[C_{43}H_{28}N_8O^{96}Ru]^{2+}$: *m/z* 384.07255, found: *m/z* 384.07322.

Preparation of $[Ru(phen)_2$salicylpip$]^{2+}$ 2. Using the same procedure as for **1** with with $[Ru(phen)_2Cl_2]$ (20 mg, 0.038 mmol) and salicylsalphen piperidine ligand (21 mg, 0.038 mmol) gave the crude product that was purified by flash chromatography on silica (CH_3CN/H_2O/ KNO_{3sat} 10:1:1/4) to provide the title compound **2** as an orange solid (35 mg, 0.029 mmol, 72%). R_f 0.32 (CH_3CN/H_2O/ KNO_{3sat} 10:1:1/2); **^{1}H NMR (CD_3CN, 500 MHz)** δ δ 9.12 – 9.03 (m, 4H, ***H$_d$*** and ***H$_c$***), 8.62 (m, 4H, ***H$_2$*** and ***H$_9$***), 8.28 (s, 4H, ***H$_5$*** and ***H$_6$***), 8.17 (d, *J* = 8.8 Hz, 2H, ***H$_e$***), 8.10 (d, *J* = 5.2 Hz, 2H, ***H$_7$***), 8.04 (dd, *J* = 5.2, 1.2 Hz, 2H, ***H$_4$***), 8.00 (d, *J* = 5.2 Hz, 2H, ***H$_a$***), 7.71 – 7.67 (m, 2H, ***H$_b$***), 7.65 (m, 4H, ***H$_3$*** and ***H$_8$***), 6.79 (d, *J* = 8.8 Hz, 2H, ***H$_f$***), 6.73 (m, 2H, ***H$_h$***), 4.43 (t, 2H, ***H$_i$***), 3.48 (broad s, 4H, ***H$_j$***), 1.30 (broad s, 4H, ***H$_m$***). **HRMS-ESI** calculated for $[C_{64}H_{60}N_{10}O_4{}^{96}Ru]^{2+}$: *m/z* 564.19320, found: *m/z* 564.19332.

Preparation of $[Ru(phen)_2$coumarin$]^{2+}$ 3. Using the same procedure as for **1** with with $[Ru(phen)_2Cl_2]$ (20 mg, 0.038 mmol) and coumarinsalphen ligand (21 mg, 0.038 mmol) gave the crude product that was purified by flash chromatography on silica (CH_3CN/H_2O/ KNO_{3sat} 10:1:1/4) to provide the title compound **3** as an orange solid (38 mg, 0.029 mmol, 77%). R_f 0.27 (CH_3CN/H_2O/ KNO_{3sat} 10:1:1/4); **^{1}H NMR (CD_3CN, 500 MHz)** δ 8.62-8.58 (m, 4H, ***H$_2$*** and ***H$_9$***), 8.26 (s, 4H, ***H$_5$*** and ***H$_6$***), 8.08 (d, *J* = 5.3, 2H, ***H$_a$***), 8.02 (m, 8H, ***H$_4$***, ***H$_7$***, ***H$_b$*** and ***H$_c$***), 7.97 (d, *J* = 9.6 Hz, 2H, ***H$_g$***), 7.71 (d, *J* = 8.7 Hz, 2H, ***H$_f$***), 7.63 (d, *J* = 4.8 Hz, 2H, m, 2H, ***H$_3$*** or ***H$_8$***), 7.60 (d, *J* = 5.2 Hz, 2H, ***H$_3$*** or ***H$_8$***), 7.14 (d, *J* = 8.7 Hz, 2H, ***H$_e$***), 6.38 (d, *J* = 9.6 Hz, 2H, ***H$_h$***). **HRMS-ESI** calculated for $[C_{52}H_{34}N_8O_6{}^{96}Ru]^{2+}$: *m/z* 505.08332, found: *m/z* 505.08356.

Preparation of $[Ru(phen)_2$quinoline$]^{2+}$ 4. Using the same procedure as for **1** with with $[Ru(phen)_2Cl_2]$ (20 mg, 0.038 mmol) and phenDK ligand (19 mg, 0.038 mmol) gave the crude product that was purified by flash chromatography on silica (CH_3CN/H_2O/ KNO_{3sat} 10:1:1/4) to provide the title compound **4** as an orange solid (38 mg, 0.030 mmol, 80%). R_f 0.29 (CH_3CN/H_2O/ KNO_{3sat} 10:1:1/4); **^{1}H NMR (CD_3CN, 500 MHz)** δ 9.28 (dd, *J* = 4.2, 1.8 Hz, 2H, ***H$_e$***), 9.18 (dd, *J* = 7.4, 1.4 Hz, 2H, ***H$_c$***), 9.12 (d, *J* = 7.7 Hz, 2H, ***H$_d$***), 8.61 – 8.59 (m, 4H, ***H$_2$*** and ***H$_9$***), 8.55 (dd, *J* = 8.4, 1.8 Hz, 2H, ***H$_g$***), 8.26 (s, 4H, ***H$_5$*** and ***H$_6$***), 8.17 (dd, *J* = 8.2, 1.3 Hz, 2H, ***H$_h$***), 8.11 (broad, 2H, ***H$_a$***), 8.03 (dd, *J* = 5.2, 1.1 Hz, 2H, ***H$_j$***), 7.98 (dd, *J* = 5.2, 1.0 Hz, 2H, ***H$_f$***), 7.90 – 7.85 (m, 2H, ***H$_i$***), 7.75 (dd, *J* = 8.3, 4.3 Hz, 2H, ***H$_b$***), 7.69 (d, *J* = 5.2 Hz, 2H, ***H$_4$*** or ***H$_7$***), 7.68 (d, *J* = 5.2 Hz, 2H, ***H$_4$*** or ***H$_7$***), 7.64 (d, *J* = 5.3 Hz, 2H, ***H$_3$*** or ***H$_8$***), 7.62 (d, *J* =

5.2 Hz, 2H, ***H*****3** or ***H*****8**). **HRMS-ESI** calculated for $[C_{56}H_{36}N_{10}{}^{96}Ru]^{2+}$: *m/z* 472.10947, found: *m/z* 472.10969.

Preparation of [Ru(phen)2Ni-salicyl]2+ 5. According to a modified procedure of Onozawa-Komatsuzaki, to a refluxing solution of $[Ru(phen)_2$diamino-phenanthroline$]^{2+}$ (20 mg, 0.021 mmol) and nickel(II) acetate tetrahydrate (6 mg, 0.025 mmol) in deoxygenated DMSO were added the salicylaldehyde (22 µL, 0.21 mmol) and triethylamine (50 µL, 0.68 mmol) .The reaction mixture was then stirred at reflux during 3 hours in the dark under argon while the solution turned from dark orange to dark red. After cooling down to room temperature, the volatiles were removed under reduced pressure. Addition of water and small portions of NH_4PF_6 led to the formation of a precipitate that was centrifuged. The crude product was purified by flash chromatography on silica (acetonitrile/water/$KNO_{3\ sat}$ with a ratio 10:1:1/2) to give compound **5** as a dark-red solid (16.4 mg, 0.0170 mmol, 64%). The counter-anion exchange from PF_6^- to Cl^- was performed by adding small portions of NBu_4Cl to a solution of the complex in acetone. **Rf** 0.32 (CH_3CN/H_2O/ KNO_{3sat} 10:1:1/2); **1H NMR (CD3CN, 500 MHz)** δ 8.76 (d, *J* = 8.5 Hz, 2H, ***H*****c**), 8.63 (d, *J* = 8.2 Hz, 2H, ***H*****4** or ***H*****7**), 8.61 (d, *J* = 8.4 Hz, 2H, ***H*****4** or ***H*****7**), 8.58 (s, 2H, ***H*****d**), 8.27 (s, 4H, ***H*****5** and ***H*****6**), 8.10 (d, *J* = 4.7 Hz, 2H, ***H*****2** or ***H*****9**), 8.03 (d, *J* = 4.9 Hz, 2H, ***H*****a**), 8.00 (d, *J* = 4.7 Hz, 2H, ***H*****2** or ***H*****9**), 7.68 (dd, *J* = 8.2, 5.2 Hz, 2H, ***H*****3** or ***H*****8**), 7.63 (dd, *J* = 8.2, 5.3 Hz, 2H, ***H*****3** or ***H*****8**), 7.59 (dd, *J* = 8.6, 5.2 Hz, 2H, ***H*****b**), 7.55 (d, *J* = 7.5 Hz, 2H, ***H*****e**), 7.40 (m, 2H, ***H*****g**), 6.92 (d, *J* = 8.9 Hz, 2H, ***H*****h**), 6.77-6.72 (m, 2H, ***H*****f**). **HRMS-ESI** calculated for $[C_{50}H_{32}N_8O_2NiRu]^{2+}$: *m/z* 468.05193, found: *m/z* 468.05215.

Preparation of [Ru(phen)2Ni-salicylpip]2+ 6. Using the same procedure as for **5** with $[Ru(phen)_2$diamino-phenanthroline$]^{2+}$ (20 mg, 0.021 mmol) and nickel(II) acetate tetrahydrate (6 mg, 0.025 mmol) in DMSO (3 mL) with the addition of 2-hydroxy-4-(2-(piperidin-1-yl)ethoxy)benzaldehyde (16 mg , 0.063 mmol) gave the crude product that was purified by flash chromatography on silica (acetonitrile/water/$KNO_{3\ sat}$ with a ratio 10:1:3/4) to yield compound **6** as a dark-red solid (15.1 mg, 0.0102 mmol, 49%). **Rf** 0.31 (CH_3CN/H_2O/ KNO_{3sat} 10:1:3/4);**1H NMR (CD3CN, 500 MHz)** δ 8.73 (d, *J* = 8.7 Hz, 2H, ***H*****c**), 8.66 (d, *J* = 8.2 Hz, 2H, ***H*****4** or ***H*****7**), 8.63 (dd, *J* = 8.3, 1.1 Hz, 2H, ***H*****4** or ***H*****7**), 8.45 (s, 2H, ***H*****d**), 8.30 (s, 4H, ***H*****5** and ***H*****6**), 8.12 (d, *J* = 4.8 Hz, 2H, ***H*****2** or ***H*****9**), 8.03 (dd, *J* = 8.9, 3.4 Hz, 4H, ***H*****a** and ***H*****2** or ***H*****9**), 7.71 (dd, *J* = 8.3, 5.3 Hz, 2H, ***H*****3** or ***H*****8**), 7.65 (dd, *J* = 8.3, 5.3 Hz, 2H, ***H*****3** or ***H*****8**), 7.59 (dd, *J* = 8.4, 5.3 Hz, 2H, ***H*****b**), 7.51 (d, *J* = 9.0 Hz, 2H, ***H*****e**), 6.48 (d, *J* = 9.0 Hz, 2H, ***H*****f**), 6.41 (broad m, 2H, ***H*****h**), 4.36 (broad m, 4H, ***H*****h**), 3.59 (broad m, 4H, ***H*****i**), 3.46 (broad m, *J* = 17.1 Hz, 4H, ***H*****j**), 3.00 (broad s, 4H, ***H*****k** and ***H*****m**), 1.30 (broad m, 4H, ***H*****l** and ***H*****m**). **HRMS-ESI** calculated for $[C_{64}H_{58}N_{10}O_4NiRu]^{2+}$: *m/z* 592.15305, found: *m/z* 592.15453.

Preparation of [Ru(phen)2Ni-coumarin]2+ 7. Using the same procedure as for **5** with $[Ru(phen)_2$diamino-phenanthroline$]^{2+}$ (20 mg, 0.021 mmol) and nickel(II) acetate tetrahydrate (6 mg, 0.025 mmol) in DMSO (3 mL) with the addition of 7-hydroxycoumarin-8-carbaldehyde (20 mg, 0.105 mmol) gave the crude product that was purified by flash chromatography on silica (acetonitrile/water/$KNO_{3\ sat}$ with a ratio 10:1:1/2) to yield compound **7** as a dark-red solid (16.7 mg, 0.0123 mmol, 59%). **Rf** 0.30 (CH_3CN/H_2O/ KNO_{3sat} 10:1:1/2);**1H NMR (CD3CN, 500 MHz)** δ 9.93 – 9.81 (broad s, 2H, ***H*****d**), 8.84 (d, *J* = 8.5 Hz, 2H, ***H*****c**), 8.68 – 8.62 (m, 4H, ***H*****4** or ***H*****7**), 8.29 (s, 4H, ***H*****5** and ***H*****6**), 8.21 (d, *J* = 4.9 Hz, 2H, ***H*****a**), 8.10 (d, *J* = 5.2 Hz, 2H, ***H*****2** or ***H*****9**), 8.05 (d, *J* = 5.0 Hz, 2H, ***H*****2** or ***H*****9**), 7.76 – 7.70 (m, 4H, ***H*****b** and ***H*****3** or ***H*****8**), 7.69 – 7.64 (m, 4H, ***H*****3** or ***H*****8** and ***H*****g**), 7.43 (d, *J* = 8.8 Hz, 2H, ***H*****f**), 6.47 (d, *J* = 9.0 Hz, 2H, ***H*****e**), 6.04 (d, *J* = 9.4 Hz, 2H, ***H*****h**). **HRMS-ESI** calculated for $[C_{52}H_{32}N_8O_6NiRu]^{2+}$: *m/z* 536.04186, found: *m/z* 536.04198.

Preparation of [Ru(phen)2Pd-salicyl]2+ 8. Using the same procedure as for **5** with $[Ru(phen)_2$diamino-phenanthroline$]^{2+}$ (20 mg, 0.021 mmol) and palladium(II) acetate (8 mg, 0.025 mmol) in DMSO (3 mL) with the addition of salicylaldehyde (22 µL, 0.21 mmol) gave the crude product that was purified by flash chromatography on silica (acetonitrile/water/$KNO_{3\ sat}$ with a ratio 10:1:1/4) to yield compound **8** as a dark-red solid (9.9 mg, 0.0077 mmol, 37%). **Rf** 0.38 (CH_3CN/H_2O/ KNO_{3sat} 10:1:1/4);**1H NMR (CD3CN, 500 MHz)** δ 8.85 (d, *J* = 8.6 Hz, 2H, ***H*****c**), 8.75 (s, 2H, ***H*****d**), 8.66 – 8.61 (m, 4H, ***H*****4** or ***H*****7**), 8.28 (s, 4H, ***H*****5** and ***H*****6**), 8.17 (dd, *J* = 5.2, 1.0 Hz, 2H, ***H*****2** or ***H*****9**), 8.08 (dd, *J* = 5.2, 0.7 Hz, 2H, ***H*****a**), 8.03 (dd, *J* = 5.2, 1.2 Hz, 2H, ***H*****2** or ***H*****9**), 7.70 (dd, *J* = 8.3, 5.3 Hz, 2H, ***H*****3** or ***H*****8**), 7.66 – 7.61 (m, 4H, ***H*****3** or ***H*****8** and ***H*****b**), 7.59 (dd, *J* = 8.1, 1.5 Hz, 2H, ***H*****e**), 7.45 – 7.40 (m, 2H, ***H*****g**), 6.92 (d, *J* = 8.7 Hz, 2H, ***H*****h**), 6.76 – 6.71 (m, 2H, ***H*****f**). **HRMS-ESI** calculated for $[C_{50}H_{32}N_8O_2PdRu]^{2+}$: *m/z* 491.53700, found: *m/z* 491.53731.

Preparation of [Ru(phen)2Pt-salicyl]2+ 9. First, $Pt(OAc)_2$ was prepared *in situ* by stirring K_2PtCl_4 (14 mg, 0.034 mmol) and NaOAc (5 mg, 0.056 mmol) in DMSO (3 mL) at 100 °C over the course of 15 minutes. Then, using the same procedure as for **5** $[Ru(phen)_2$diamino-phenanthroline$]^{2+}$ (20 mg, 0.021 mmol) and salicylaldehyde (22 µL, 0.21 mmol) were added which gave the crude product that was purified by flash chromatography on silica (acetonitrile/water/$KNO_{3\ sat}$ with a ratio 10:1:1/4) to yield compound **9** as a dark-red solid (11 mg, 0.0081 mmol, 36%). **Rf** 0.34 (CH_3CN/H_2O/ KNO_{3sat} 10:1:1/4); **1H NMR (CD3CN, 500 MHz)** δ 9.36 (s, 2H, ***H*****d**), 8.97 (d, *J* = 8.7 Hz, 2H, ***H*****c**), 8.86 (d, *J* = 8.5 Hz, 2H, ***H*****2** or ***H*****9**), 8.61 (d, *J* = 8.3 Hz, 2H, ***H*****4** or ***H*****7**), 8.58 (d, *J* = 8.3 Hz, 2H, ***H*****4** or ***H*****7**), 8.25 (s, 4H, ***H*****5** and ***H*****6**), 8.14 (dd, *J* = 5.3, 1.1 Hz, 2H, ***H*****2** or ***H*****9**), 8.10 (dd, *J* = 8.3, 1.1 Hz, ***H*****3** or ***H*****8**), 7.87 (dd, *J* = 8.1, 1.5 Hz, 2H, ***H*****e**), 7.70 – 7.50 (m, 8H, ***H*****3** or ***H*****8, H*****g** and ***H*****h**), 7.42 (dd, *J* = 8.8, 5.1 Hz, 2H, ***H*****b**), 7.38 (d, *J* = 8.5 Hz, 2H, ***H*****a**), 6.98 – 6.92 (m, 2H, ***H*****h**). **HRMS-ESI** calculated for $[C_{50}H_{32}N_8O_2PtRu]^{2+}$: *m/z* 532.07165, found: *m/z* 532.07345.

Preparation of [Ru(phen)2Pt-salicylpip]2+ 10. First, $Pt(OAc)_2$ was prepared *in situ* by stirring K_2PtCl_4 (14 mg, 0.034 mmol) and NaOAc (5 mg, 0.056 mmol) in DMSO (3 mL) at 100 °C over the course of 15 minutes. Then, using the same procedure as for **5** [Ru(phen)2di-amino-phenanthroline]$^{2+}$ (20 mg, 0.021 mmol), 2-hydroxy-4-(2-(piperidin-1-yl)ethoxy)benzaldehyde (16 mg , 0.063 mmol) which gave the crude product that was purified by flash chromatography on silica (acetonitrile/water/$KNO_{3\ sat}$ with a ratio 10:1:3/4) to yield the title compound **10** as a dark-red solid (9.4 mg, 0.0058 mmol, 28%). Rf 0.31 (CH_3CN/H_2O/ KNO_{3sat} 10:1:3/4); **1H NMR (CD3CN, 500 MHz)** δ 8.70 (d, *J* = 8.7 Hz, 2H, ***H*****c**), 8.63 (d, *J* = 8.2 Hz, 4H, ***H*****2** and ***H*****9**), 8.60 (dd, *J* = 8.3, 1.1 Hz, 2H), 8.42 (s, 2H, ***H*****d**), 8.26 (s, 4H, ***H*****5** and ***H*****6**), 8.09 (d, *J* = 4.8 Hz, 2H, ***H*****4** or ***H*****7**), 8.00 (dd, *J* = 8.9, 3.4 Hz, 4H, ***H*****a** and ***H*****4** or ***H*****7**), 7.68 (dd, *J* = 8.3, 5.3 Hz, 2H, ***H*****3** or ***H*****8**), 7.62 (dd, *J* = 8.3, 5.3 Hz, 2H, ***H*****b**), 7.56 (dd, *J* = 8.4, 5.3 Hz, 2H, ***H*****b**), 7.48 (d, *J* = 9.0 Hz, 2H, ***H*****e**), 6.45 (d, *J* = 9.0 Hz, 2H, ***H*****f**), 6.38 (s, 2H, ***H*****h**), 4.33 (broad s, 4H, ***H*****i**), 3.61 (broad s, 4H, ***H*****k**), 3.49 (broad s, *J* = 17.1 Hz, 4H, ***H*****j**), 3.03 (broad s, 4H, ***H*****l**), 1.33 (broad s, 4H, ***H*****m**). **HRMS-ESI** calculated for $[C_{64}H_{58}N_{10}O_4{}^{190}Pt^{96}Ru]^{2+}$: *m/z* 659.6667, found: *m/z* 659.6683.

Electrochemical studies

Cyclic voltammetry was carried out in a one-compartment cell, using a glassy carbon disk working electrode (approximate area 0.03 cm^2), a platinum wire counter electrode, and an Ag/AgCl reference electrode. The potential of the working electrode was controlled by an Autolab PGSTAT 100 potentiostat through a PC interface. Cyclic voltammograms were recorded at a sweep rate of 100 mVs^{-1} from solutions in dry acetonitrile (Sigma–Aldrich, HPLC grade). The concentration of the complexes was $8x10^{-4}$ mol L^{-1}, with 0.1 mol L^{-1} tetrabutylammonium perchlorate as supporting electrolyte. Before each measurement, the samples were purged with nitrogen. Redox potentials were determined by comparison with ferrocene, added at the end of the measurement. Luminescence titration experiments with ODNs (GC-rich hairpin or wtTel23 G-quadruplex DNA) were conducted by recording spectra from solutions in 10 mM HEPES, 50 mM NaCl, 100 mM KCl (pH 7.4) buffer on a Varian Cary Eclipse instrument. Titrations were performed by starting from the highest DNA concentration and progressively decreasing it, whilst the concentration of the complex (5 µm) was kept constant.

Photophysical measurments

UV/Vis absorption spectra were recorded on a Shimadzu UV-1700 spectrophotometer. Room temperature luminescence spectra were recorded on a Varian Cary Eclipse instrument. Luminescence intensity at 77 K was recorded on a FluoroLog 3 FL3-22 from Jobin Yvon equipped with an 18 V 450 W short-arc xenon lamp and an R928P photomultiplier, using an Oxford Instruments Optistat DN nitrogen cryostat controlled by an Oxford Intelligent Temperature Controller (ITC503S). Quantum yields were obtained using $[Ru(bpy)_3]^{2+}$ as a reference.[47] Luminescence lifetime measurements were performed after irradiation at λ=450 nm obtained as the second harmonic of a titanium: sapphire laser (picosecond Tsunami laser Spectra at a repetition rate of 80 kHz. A Fluotime 200 instrument from AMS Technologies was used for the decay acquisition. It consists of a GaAs microchannel plate photomultiplier tube (Hamamatsu model R3809U-50) followed by a time-correlated single-photon counting system from Picoquant (PicoHarp300). The ultimate time resolution of the system is close to 4 ps. Luminescence decays were analyzed with FLUOFIT software available from Picoquant.

CD experiments

Prior to CD analysis, oligonucleotides were annealed by heating at 95 °C for 5 min in buffered medium, then allowed to cool to room temperature overnight. Spectra were recorded on a JASCO J-810 spectropolarimeter from solutions in 1 cm path length quartz cuvettes at 5 °C increments from 25 °C to 95 °C over the wavelength range from 230 to 330 nm. At each temperature, the spectrum was an average of three scans with response time 0.5 s, data pitch 1 nm, bandwidth 4 nm, and scanning speed 200 $nmmin^{-1}$. For CD melting experiments, the ellipticity was recorded at 292 and 252 nm for wtTel23 and duplex hairpin, respectively. Melting temperatures were obtained through Boltzmann fitting with Origin software. Each curve fit was only accepted with r^2>0.99.

Bio-layer interferometry

Bio-layer interferometry experiments were performed using sensors coated with streptavidin (SA sensors) purchased from Forte Bio (PALL). Prior to use, they were immersed for 10 minutes in a buffer before functionalization to dissolve the sucrose layer. Then the sensors were dipped for 15 minutes in DNA containing solutions (biotinylated hairpin oligonucleotides) at 100 nM and rinsed in the buffer solution (10 mM HEPES, 50 mM NaCl, 100 mM KCl (pH 7.4), 0.5% v/v surfactant P20) for 10 minutes. The functionalized sensors were next dipped in the ruthenium complex containing solution at different concentrations (see supporting information) for 2 minutes interspersed by a rinsing step in the buffer solution for 4 minutes. Reference sensors without DNA immobilization were used to subtract the non-specific adsorption on the SA layer. The sensorgrams were fit using a 1 : 1 interaction model. The reported values are the means of representative independent experiments, and the errors provided are standard deviations from the mean. Each experiment was repeated at least two times.

Confocal laser scanning microscopy

U2OS cells were grown at 37 °C in a humidified atmosphere with 5% CO_2 in DMEM medium (Westburg) containing 10% foetal bovine serum (FBS) (Gibco) and 1% penicillin/streptomycin (Westburg). 20000 cells were seeded onto a coated microscope slide and incubated with 20 µM of complex for 1,5 h in the dark. After incubation, the medium containing the complex was removed, and fresh medium was added to the cells. The cells were rinsed in pre-warmed PBS, fixed in 4% paraformaldehyde (VWR) for 10 min, and labelled with DRAQ5 (eBioscience) following the instructions of the manufacturer. A confocal laser scanning microscopy system (Zeiss LSM 710) was used to acquire the images, which were processed with Zen software.

Photo-cytotoxicity experiments

U2OS cells were cultured for 24 h in DMEM (Westburg) containing 10% FBS (Gibco) and 1% penicillin/streptomycin (Westburg) in 96-well plates to reach a density of 10000 cells/well. The supernatant was then removed and fresh medium containing the complex was added. After one hour of incubation at 37 °C in the dark, cells were rinsed twice with 1x PBS to remove non-internalized complex. They were then illuminated for 30 min with blue LEDs (LED strip IP68 60 $LEDm^{-1}$ from Prolumia, 405 nm at 15.7 Wm^{-2}). The distance between the light source and the culture plate was 10 cm. Cultures were rinsed with 1x PBS before illumination still in 1x PBS to avoid absorption by red phenol-containing culture medium. Dark controls were protected from illumination with aluminium foil. Illuminated and control cultures were directly put back in the incubator after addition of fresh medium and incubated for another 24 hours. Cell viability was measured 1 day post-irradiation using 10 µL/well of WST-1 reagent (Roche) following the manufacturer's instructions. The ratio of the optical density at λ=450 nm under each set of conditions to that of control cells (non-transfected and non-irradiated, 100% viability) was used to determine the relative viability. Experiments were performed in triplicate with 4 measurements each time.

Acknowledgements

M. G., J. W. and B. E. gratefully acknowledge the Université catholique de Louvain (UCLouvain), the Fonds National pour la Recherche Scientifique (F.R.S.-F.N.R.S.) and the Prix Pierre et Colette Bauchau for financial support. We also thank Simon De Kreijger and Robin Bevernaegie for their scientific support. This work was partially supported by the"Agence National de la Recherche", Labex ARCANE (ANR-16-CE11-0006-01), CBH-EUR-GS (ANR-17-EURE-0003), and the région Auvergne-Rhône-Alpes. The NanoBio-ICMG platforms (FR 2607) are acknowledged for their support.

Keywords: G-quadruplex DNA • Ruthenium complexes • Schiff base • Photo-cytotoxicity • Bio-layer interferometry

References

[1] A. Gilman, F. S. Philips, *Science* **1946**, *103*, 409-436.
[2] L. H. Hurley, *Nat. Rev. Cancer* **2002**, *2*, 188-200.
[3] A. Granzhan, N. Kotera, M.-P. Teulade-Fichou, *Chem. Soc. Rev.* **2014**, *43*, 3630-3665.
[4] Q. Deraedt, L. Marcélis, T. Auvray, G. S. Hanan, F. Loiseau, B. Elias, *Eur. J. Inorg. Chem.* **2016**, *2016*, 3649-3658.
[5] D. M. Hyman, B. S. Taylor, J. Baselga, *Cell* **2017**, *168*, 584-599.
[6] Q. Deraedt, L. Marcelis, F. Loiseau, B. Elias, *Inorg. Chem. Front.* **2017**, *4*, 91-103.
[7] M. Gillard, B. Laramée-Milette, Q. Deraedt, G. S. Hanan, F. Loiseau, J. Dejeu, E. Defrancq, B. Elias, L. Marcélis, *Inorg. Chem. Front.* **2019**, *6*, 2260-2270.
[8] D. Drygin, A. Siddiqui-Jain, S. O'Brien, M. Schwaebe, A. Lin, J. Bliesath, C. B. Ho, C. Proffitt, K. Trent, J. P. Whitten, J. K. C. Lim, D. Von Hoff, K. Anderes, W. G. Rice, *Cancer Res.* **2009**, *69*, 7653-7661.
[9] H. Xu, M. Di Antonio, S. McKinney, V. Mathew, B. Ho, N. J. O'Neil, N. D. Santos, J. Silvester, V. Wei, J. Garcia, F. Kabeer, D. Lai, P. Soriano, J. Banáth, D. S. Chiu, D. Yap, D. D. Le, F. B. Ye, A. Zhang, K. Thu, J. Soong, S.-c. Lin, A. H. C. Tsai, T. Osako, T. Algara, D. N. Saunders, J. Wong, J. Xian, M. B. Bally, J. D. Brenton, G. W. Brown, S. P. Shah, D. Cescon, T. W. Mak, C. Caldas, P. C. Stirling, P. Hieter, S. Balasubramanian, S. Aparicio, *Nat. Commun.* **2017**, *8*, 14432.
[10] H. Han, L. H. Hurley, *Trends Pharmacol. Sci.* **2000**, *21*, 136-142.
[11] S. Burge, G. N. Parkinson, P. Hazel, A. K. Todd, S. Neidle, *Nucleic Acids Res.* **2006**, *34*, 5402-5415.
[12] C.-R. Graziella, Z. Nadia, F. Marco, *Curr. Pharm. Des.* **2016**, *22*, 6612-6624.
[13] T. de Lange, L. Shiue, R. M. Myers, D. R. Cox, S. L. Naylor, A. M. Killery, H. E. Varmus, *Mol. Cell. Biol.* **1990**, *10*, 518-527.
[14] A. L. Moye, K. C. Porter, S. B. Cohen, T. Phan, K. G. Zyner, N. Sasaki, G. O. Lovrecz, J. L. Beck, T. M. Bryan, *Nat. Commun.* **2015**, *6*, 7643.
[15] A. De Cian, L. Lacroix, C. Douarre, N. Temime-Smaali, C. Trentesaux, J.-F. Riou, J.-L. Mergny, *Biochimie* **2008**, *90*, 131-155.
[16] C. Javier, A. R. Martin, N. Stephen, *Mini-Rev. Med. Chem.* **2003**, *3*, 11-21.
[17] G. Biffi, D. Tannahill, J. Miller, W. J. Howat, S. Balasubramanian, *PLoS One* **2014**, *9*, e102711.
[18] M.-P. Teulade-Fichou, C. Carrasco, L. Guittat, C. Bailly, P. Alberti, J.-L. Mergny, A. David, J.-M. Lehn, W. D. Wilson, *J. Am. Chem. Soc.* **2003**, *125*, 4732-4740.
[19] M. J. B. Moore, C. M. Schultes, J. Cuesta, F. Cuenca, M. Gunaratnam, F. A. Tanious, W. D. Wilson, S. Neidle, *J. Med. Chem.* **2006**, *49*, 582-599.
[20] A. De Cian, E. DeLemos, J.-L. Mergny, M.-P. Teulade-Fichou, D. Monchaud, *J. Am. Chem. Soc.* **2007**, *129*, 1856-1857.
[21] I. M. Dixon, F. Lopez, A. M. Tejera, J.-P. Estève, M. A. Blasco, G. Pratviel, B. Meunier, *J. Am. Chem. Soc.* **2007**, *129*, 1502-1503.
[22] J. Jamroskovic, M. Doimo, K. Chand, I. Obi, R. Kumar, K. Brännström, M. Hedenström, R. Nath Das, A. Akhunzianov, M. Deiana, K. Kasho, S. Sulis Sato, P. L. Pourbozorgi, J. E. Mason, P. Medini, D. Öhlund, S. Wanrooij, E. Chorell, N. Sabouri, *J. Am. Chem. Soc.* **2020**.
[23] C. Romera, O. Bombarde, R. Bonnet, D. Gomez, P. Dumy, P. Calsou, J. F. Gwan, J. H. Lin, E. Defrancq, G. Pratviel, *Biochimie* **2011**, *93*, 1310-1317.
[24] A. Pipier, A. De Rache, C. Modeste, S. Amrane, E. Mothes-Martin, J.-L. Stigliani, P. Calsou, J.-L. Mergny, G. Pratviel, D. Gomez, *Dalton Trans.* **2019**, *48*, 6091-6099.
[25] N. H. Abd Karim, O. Mendoza, A. Shivalingam, A. J. Thompson, S. Ghosh, M. K. Kuimova, R. Vilar, *RSC Advances* **2014**, *4*, 3355-3363.
[26] A. Łęczkowska, J. Gonzalez-Garcia, C. Perez-Arnaiz, B. Garcia, A. J. P. White, R. Vilar, *Chem. Eur. J.* **2018**, *24*, 11785-11794.
[27] L. Lecarme, E. Prado, A. De Rache, M.-L. Nicolau-Travers, R. Bonnet, A. v. D. Heyden, C. Philouze, D. Gomez, J.-L. Mergny, H. Jamet, E. Defrancq, O. Jarjayes, F. Thomas, *Inorg. Chem.* **2014**, *53*, 12519-12531.
[28] L. Lecarme, E. Prado, A. De Rache, M.-L. Nicolau-Travers, G. Gellon, J. Dejeu, T. Lavergne, H. Jamet, D. Gomez, J.-L. Mergny, E. Defrancq, O. Jarjayes, F. Thomas, *ChemMedChem* **2016**, *11*, 1133-1136.
[29] S. Bandeira, J. Gonzalez-Garcia, E. Pensa, T. Albrecht, R. Vilar, *Angew. Chem. Int. Ed. Engl.* **2018**, *57*, 310-313.
[30] G. Piraux, L. Bar, M. Abraham, T. Lavergne, H. Jamet, J. Dejeu, L. Marcélis, E. Defrancq, B. Elias, *Chem. Eur. J.* **2017**, *23*, 11872-11880.
[31] J. Weynand, A. Diman, M. Abraham, L. Marcélis, H. Jamet, A. Decottignies, J. Dejeu, E. Defrancq, B. Elias, *Chem. Eur. J.* **2018**, *24*, 19216-19227.
[32] Q. Cao, Y. Li, E. Freisinger, P. Z. Qin, R. K. O. Sigel, Z.-W. Mao, *Inorg. Chem. Front.* **2017**, *4*, 10-32.
[33] S. Asamitsu, T. Bando, H. Sugiyama, *Chem. Eur. J.* **2019**, *25*, 417-430.
[34] B. Prasad, J. Jamroskovic, S. Bhowmik, R. Kumar, T. Romell, N. Sabouri, E. Chorell, *Chem. Eur. J.* **2018**, *24*, 7926-7938.
[35] H. Ihmels, M. Karbasiyoun, K. Löhl, C. Stremmel, *Org. Biomol. Chem.* **2019**, *17*, 6404-6413.
[36] A. B. Tossi, J. M. Kelly, *Photochem. Photobiol.* **1989**, *49*, 545-556.
[37] S. M. Cloonan, R. B. P. Elmes, M. Erby, S. A. Bright, F. E. Poynton, D. E. Nolan, S. J. Quinn, T. Gunnlaugsson, D. C. Williams, *J. Med. Chem.* **2015**, *58*, 4494-4505.
[38] F. E. Poynton, S. A. Bright, S. Blasco, D. C. Williams, J. M. Kelly, T. Gunnlaugsson, *Chem. Soc. Rev.* **2017**, *46*, 7706-7756.
[39] C. J. Cardin, J. M. Kelly, S. J. Quinn, *Chem. Sci.* **2017**, *8*, 4705-4723.
[40] O.-K. Nobuko, K. Ryuzi, H. Yuichiro, S. Hideki, A. Hironori, K. Kazuyuki, *Bull. Chem. Soc. Jpn.* **2003**, *76*, 977-984.
[41] J. Bolger, A. Gourdon, E. Ishow, J.-P. Launay, *Inorg. Chem.* **1996**, *35*, 2937-2944.
[42] Y. Pellegrin, A. Quaranta, P. Dorlet, M. F. Charlot, W. Leibl, A. Aukauloo, *Chem. Eur. J.* **2005**, *11*, 3698-3710.
[43] Y.-Y. Lin, S.-C. Chan, M. C. W. Chan, Y.-J. Hou, N. Zhu, C.-M. Che, Y. Liu, Y. Wang, *Chem. Eur. J.* **2003**, *9*, 1263-1272.
[44] C.-M. Che, S.-C. Chan, H.-F. Xiang, M. C. W. Chan, Y. Liu, Y. Wang, *Chem. Commun.* **2004**, 1484-1485.
[45] A. Boisdenghien, C. Moucheron, A. Kirsch-De Mesmaeker, *Inorg. Chem.* **2005**, *44*, 7678-7685.
[46] A. M. López, M. Natali, E. Pizzolato, C. Chiorboli, M. Bonchio, A. Sartorel, F. Scandola, *Phys. Chem. Chem. Phys.* **2014**, *16*, 12000-12007.
[47] A. M. Brouwer, *Pure Appl. Chem.* **2011**, *83*, 2213-2228.
[48] A. E. Friedman, J. C. Chambron, J. P. Sauvage, N. J. Turro, J. K. Barton, *J. Am. Chem. Soc.* **1990**, *112*, 4960-4962.
[49] J. Kypr, I. Kejnovská, D. Renciuk, M. Vorlícková, *Nucleic Acids Res.* **2009**, *37*, 1713-1725.
[50] M. P. O'Hagan, J. C. Morales, M. C. Galan, *European J. Org. Chem.* **2019**, *0*.
[51] P. Murat, Y. Singh, E. Defrancq, *Chem. Soc. Rev.* **2011**, *40*, 5293-5307.
[52] J. Wallner, G. Lhota, D. Jeschek, A. Mader, K. Vorauer-Uhl, *J. Pharm. Biomed. Anal.* **2013**, *72*, 150-154.
[53] J. Weynand, H. Bonnet, F. Loiseau, J.-L. Ravanat, J. Dejeu, E. Defrancq, B. Elias, *Chem. Eur. J.* **2019**, *25*, 12730-12739.

Entry for the Table of Contents

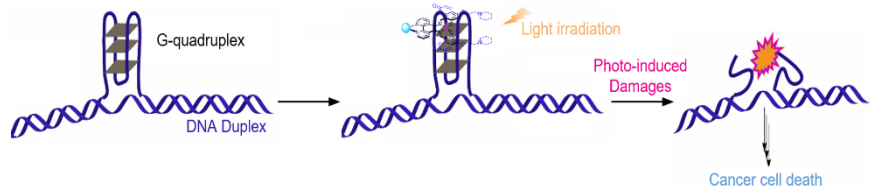

Ruthenium(II) Schiff base complexes are relevant compounds for G-quadruplex DNA binding and display interesting photo-cytotoxicity properties.